nature chemistry

Article

https://doi.org/10.1038/s41557-023-01138-9

Nanoparticle stereochemistry-dependent endocytic processing improves in vivo mRNA delivery

Received: 4 October 2021

Accepted: 13 January 2023

Published online: 02 March 2023

Check for updates

Marine Z. C. Hatit[1,6], Curtis N. Dobrowolski[1,6], Melissa P. Lokugamage[1], David Loughrey[1], Huanzhen Ni[1], Chiara Zurla[2], Alejandro J. Da Silva Sanchez[1], Afsane Radmand[1], Sebastian G. Huayamares[1], Ryan Zenhausern[1], Kalina Paunovska[1], Hannah E. Peck[2], Jinwhan Kim[1,3], Manaka Sato[1], Jacob I. Feldman[1], Michael-Alexander Rivera[1], Ana Cristian[1], YongTae Kim[1,2,4,5], Philip J. Santangelo[1] & James E. Dahlman[1]

Stereochemistry can alter small-molecule pharmacokinetics, safety and efficacy. However, it is unclear whether the stereochemistry of a single compound within a multicomponent colloid such as a lipid nanoparticle (LNP) can influence its activity in vivo. Here we report that LNPs containing stereopure 20α-hydroxycholesterol (20α) delivered mRNA to liver cells up to 3-fold more potently than LNPs containing a mixture of both 20α- and 20β-hydroxycholesterols (20mix). This effect was not driven by LNP physiochemical traits. Instead, in vivo single-cell RNA sequencing and imaging revealed that 20mix LNPs were sorted into phagocytic pathways more than 20α LNPs, resulting in key differences between LNP biodistribution and subsequent LNP functional delivery. These data are consistent with the fact that nanoparticle biodistribution is necessary, but not sufficient, for mRNA delivery, and that stereochemistry-dependent interactions between LNPs and target cells can improve mRNA delivery.

The spatial arrangement of a given chemical group within a small-molecule drug—referred to as its stereochemistry—affects drug activity and safety[1]. One well-known example relating stereochemistry to drug activity is thalidomide, a molecule formerly prescribed for morning sickness[2]. This and other examples[3,4] have led scientists to conclude that isolating the active and safe isomer from an impure mixture can improve drug efficacy. Given the abundance of stereochemistry-dependent protein interactions[5,6] and the fact that in vivo drug delivery requires nanoparticle–protein interactions in serum[7], at the cell surface[8–12], within endosomes[9–12] and within the cytoplasm[13], we hypothesized that lipid nanoparticle (LNP) stereochemistry impacted LNP-mediated mRNA delivery. This hypothesis has clinical relevance[14]; LNPs have safely delivered disease-modifying siRNA[15] and mRNA[16–18] in patients, highlighting the potential impact of a design rule to improve LNP efficacy.

Results

Stereochemistry affects LNP-mediated mRNA delivery

To test this hypothesis, we focused on cKK-E12, a six-stereocentre lipopeptide (Fig. 1a) that exhibits selective siRNA and mRNA delivery to non-human primates at low doses[19]. Using the synthetic strategy previously described[19] produces several diastereomers, the ratio of which is

[1]Wallace H. Coulter Department of Biomedical Engineering, Georgia Institute of Technology and Emory University School of Medicine, Atlanta, GA, USA. [2]Parker H. Petit Institute for Bioengineering and Bioscience, Georgia Institute of Technology, Atlanta, GA, USA. [3]School of Electrical & Computer Engineering, Georgia Institute of Technology, Atlanta, GA, USA. [4]George W. Woodruff School of Mechanical Engineering, Georgia Institute of Technology, Atlanta, GA, USA. [5]Institute for Electronics and Nanotechnology, Georgia Institute of Technology, Atlanta, GA, USA. [6]These authors contributed equally: Marine Z. C. Hatit, Curtis N. Dobrowolski. e-mail: james.dahlman@emory.edu

https://doi.org/10.1038/s41557-023-01138-9

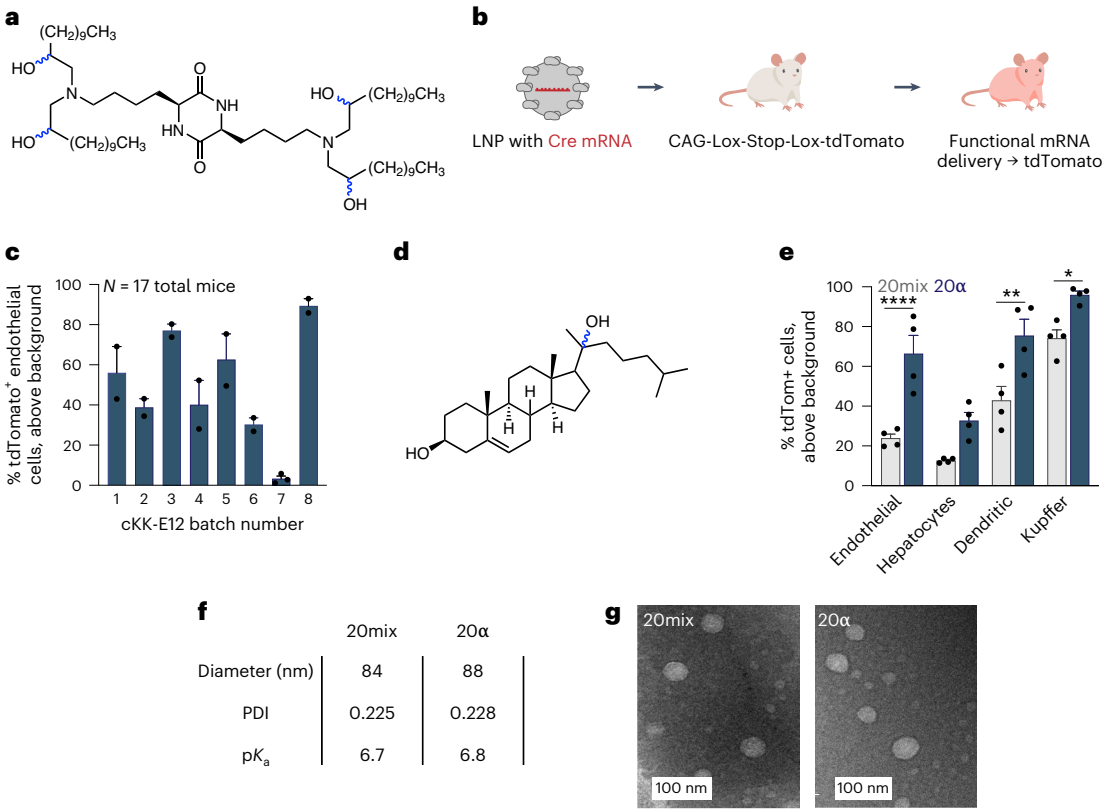

	20mix	20α
Diameter (nm)	84	88
PDI	0.225	0.228
pK_a	6.7	6.8

Fig. 1 | In vivo LNP-mediated mRNA delivery varies batch-to-batch. a, cKK-E12 chemical structure with undefined stereocentres highlighted in blue. **b**, LNPs were formulated to carry chemically modified mRNA encoding Cre recombinase and intravenously administered to Ai14 mice at 0.3 mg per kg (body weight). Cells within Ai14 mice contain a CAG-Lox-Stop-Lox-tdTomato construct. These cells become tdTomato$^+$ (tdTom$^+$) when Cre mRNA is delivered into the cytoplasm and translated into the functional Cre protein, which edits the genome by excising the Stop cassette. **c**, The percentage of tdTom$^+$ cells, measured by flow cytometry, 3 days after injection with eight batches of cKK-E12 carrying Cre mRNA. $n = 2–3$ per group. **d**, 20-Hydroxycholesterol chemical structure with stereocentre highlighted in blue. **e**, The percentage of tdTom$^+$ cells, measured by flow cytometry, 3 days after Ai14 mice were injected with 0.3 mg per kg (body weight) of LNPs formulated with 20α or 20mix. The 20α LNPs led to more tdTom$^+$ cells than 20mix LNPs. $n = 4$ per group, average ± s.e.m., two-way analysis of variance (ANOVA), $^*P = 0.04$, $^{**}P = 0.0014$, $^{****}P < 0.0001$. **f,g**, When we compared 20α- and 20mix-containing LNPs, the difference in LNP-mediated mRNA delivery was not explained by LNP hydrodynamic diameter, polydispersity index (PDI) or pK_a (**f**) or morphology (**g**). $n = 3$ per group, average ± s.d.

likely to vary batch-to-batch. Since cKK-E12 is the most prominent component of the LNP, we postulated that if stereochemistry impacts LNP efficacy, then different batches of cKK-E12 could exhibit different levels of LNP delivery. We synthesized and purified eight batches of cKK-E12 using the same synthetic strategy and formulated them into LNPs using microfluidics[20] to carry chemically modified mRNA encoding Cre recombinase (Cre) (Fig. 1a,b). As a control to ensure that the effects were due to cKK-E12 batch differences, we formulated the LNPs using the same batch of 20α-hydroxycholesterol (20α), $C_{18}PEG_{2K}$ (PEG, polyethylene glycol) and 1,2-dioleoyl-*sn*-glycero-3-phosphoethanolamine (DOPE). As a second control, we mixed the cKK-E12, 20α, $C_{18}PEG_{2K}$ and DOPE in a 50:35:2.5:12.5 molar ratio, which had been previously characterized[21].

We intravenously administered the eight batches to Ai14 mice at the clinically relevant dose[15,16] of 0.3 mg per kg (body weight). Since cells within Ai14 mice contain a CAG-Lox-Stop-Lox-tdTomato construct, these cells become tdTomato$^+$ (tdTom$^+$) when Cre mRNA is delivered into the cytoplasm and is translated into the functional Cre protein, which edits the genome by excising the Stop cassette[22] (Fig. 1b). Three days after injection, we quantified the percentage of tdTom$^+$ liver non-parenchymal cells and hepatocytes using flow cytometry (Supplementary Fig. 1). We observed batch-dependent LNP efficacy (Fig. 1c). We reasoned that batch-dependent delivery could be caused by overt differences in LNP biophysical traits. However, LNP hydrodynamic diameter and polydispersity were consistent (Supplementary Fig. 2). One plausible explanation is that the relative abundance of the diastereomers influenced delivery. Nonetheless, the complexity of the cKK-E12 mixture did not allow us to quantify the diastereomers present in the different batches; thus, while these data could be driven by stereochemistry, they were not conclusive.

These data led us to test our hypothesis using a stereochemistry model system. Specifically, we focused on a 20-hydroxycholesterol -based LNP that delivered mRNA at clinically relevant doses to liver cells[21]. Notably, 20-hydroxycholesterol exists in only two conformations, 20α and 20β, thereby allowing us to isolate the effect of stereochemistry (Fig. 1d). Three days after injecting 20α LNPs carrying Cre mRNA, we found that this LNP delivered Cre mRNA at a 0.025 mg per kg (body weight) dose to multiple liver non-parenchymal cells (Supplementary Fig. 3). We then formulated LNPs carrying Cre mRNA and 20α or a mixture of 20α and 20β at an ~2:1 molar ratio (20mix). We injected the LNPs at a dose of 0.3 mg per kg (body weight) into Ai14 mice, with phosphate-buffered saline (PBS) as a control, and quantified the percentage of tdTom$^+$ cells using flow cytometry three days later. LNPs containing 20α resulted in a higher percentage of tdTom$^+$ cells than LNPs containing 20mix (Fig. 1e); these differences were statistically significant in endothelial cells, dendritic cells and Kupffer cells, and were insignificantly increased in hepatocytes ($P = 0.067$). When we compared 20α- and 20mix-containing LNPs, the difference in LNP-mediated mRNA delivery was not explained by LNP stability in mouse serum (Supplementary Fig. 4) or LNP hydrodynamic diameter, polydispersity,

https://doi.org/10.1038/s41557-023-01138-9

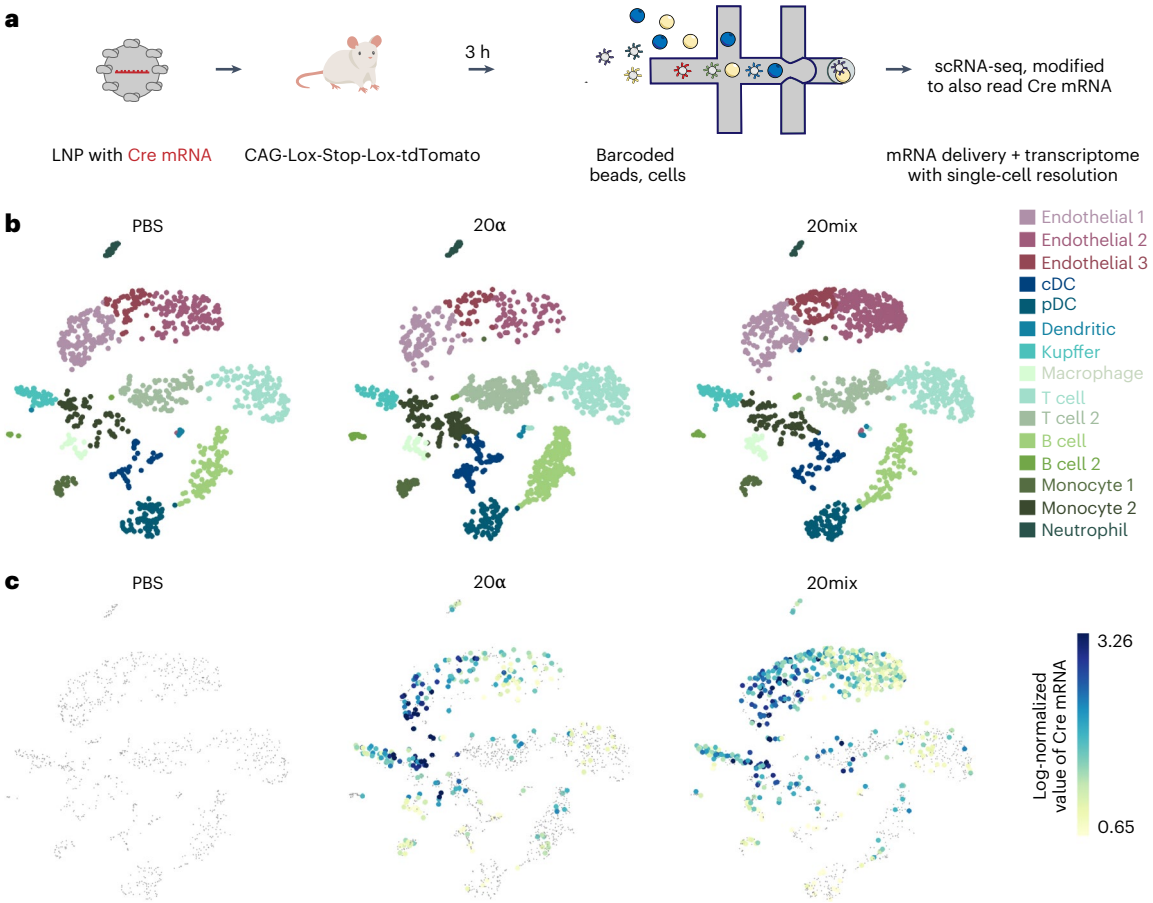

Fig. 2 | Quantifying in vivo LNP-mediated mRNA delivery at single-cell resolution. a, LNPs were formulated to carry chemically modified mRNA encoding Cre recombinase and intravenously administered to Ai14 mice at 0.3 mg per kg (body weight). Three hours after systemically injecting mice with PBS, 20α LNPs or 20mix LNPs, liver non-parenchymal cells were isolated using FACS. scRNA-Seq was then performed using the 10X Chromium System, ~2,000 cells were loaded per condition and the resulting data were processed using Cell Ranger. **b**, t-SNE plots of mice treated with PBS, 20α LNPs or 20mix LNPs. BBrowser was used to associate each cluster with a specific cell type. cDC, conventional dendritic cells; pDC, plasmacytoid dendritic cells. **c**, The amount of Cre mRNA delivered in each cell overlaid on the t-SNE plots. Small grey dots represent cells with no measured delivery.

pK_a or morphology (Fig. 1f,g). These data provide one line of evidence that LNP stereochemistry affects mRNA delivery in vivo.

Quantifying in vivo LNP-mediated mRNA delivery at single-cell resolution

We then investigated the biological mechanism that could be responsible for increased delivery mediated by 20α LNPs, relative to 20mix LNPs. Inspired by recent data demonstrating that cells exhibit enantiomer-specific transcriptomic responses to small molecules[23,24], we reasoned that analysing the transcriptional response of liver non-parenchymal cells to 20α and 20mix LNPs using single-cell RNA sequencing (scRNA-Seq) could provide insights into the relationship between cell state and delivery.

Three hours after systemically injecting mice with PBS, 20α LNPs carrying 0.3 mg per kg (body weight) Cre mRNA, or 20mix LNPs carrying 0.3 mg per kg (body weight) Cre mRNA, we isolated liver non-parenchymal cells using fluorescence-activated cell sorting (FACS) (Fig. 2a). We then performed scRNA-Seq using the 10X Chromium System (Fig. 2a), loaded ~2,000 cells per condition and processed the resulting data using Cell Ranger. The mapping rate and average read depth of ~100,000 reads per cell (Supplementary Fig. 5) were comparable to reported scRNA-Seq experiments[25–29]. For all three conditions, unsupervised clustering partitioned the ~1,600 cells into 15 clusters (Fig. 2b). The clustering distribution was similar in all three conditions, indicating that new cell subpopulations were not formed when mice were treated with LNPs. We then used *t*-distributed stochastic neighbour embedding (t-SNE) to visualize the expression of shared highly variable genes within the clusters (Fig. 2b). This approach identified cell subtypes within the liver that are usually not easily identified using flow cytometry.

It is important to understand LNP on- and off-target delivery in vivo; this is often characterized using luminescence or immunofluorescence. However, these techniques are not suitable for quantifying delivery in single cells or cell subtypes. To obtain single-cell resolution of mRNA delivery, we developed an scRNA-seq workflow to quantify Cre mRNA delivered by the LNPs in single cells, along with the cell transcriptome (Fig. 2c). Specifically, we classified the Cre mRNA sequence as an artificial gene in Cell Ranger and measured it alongside the endogenous mRNA. As a negative control, we found no Cre mRNA in PBS-treated mice, suggesting that Cre sequencing reads in Cre mRNA-treated mice were not due to sequencing errors. As a second control, we compared Cre mRNA delivery to the percentage of tdTom$^+$ cells. For both LNP-treated conditions, Cre mRNA reads were highest in Kupffer and endothelial cells, which was consistent with the functional delivery profile observed with flow cytometry (Fig. 1e). This assay led to a surprising observation: an increase in mRNA reads for cells from mice treated with 20mix LNPs, compared to cells from mice treated with 20α LNPs (Fig. 2c and Supplementary Fig. 6). Thus, at the 3 h time

point, there was more Cre mRNA present in the 20mix cells, relative to 20α, even though we observed up to 3-fold less tdTomato protein in the 20mix cells, relative to 20α, three days postinjection (Fig. 1e). These data suggest that the stereochemistry-dependent increase in Cre mRNA biodistribution did not lead to subsequent increased Cre protein activity.

The in vivo transcriptional response to LNPs

Previous data led us to hypothesize that the difference between Cre mRNA biodistribution and downstream Cre protein activity could be explained by cellular responses that affected (1) endocytosis pathways[30–32], (2) maturation into late endosomes[32,33], (3) phagocytosis and lysosomal degradation[12], or (4) protein translation efficacy. We therefore performed a differential expression analysis comparing both 20α and 20mix LNP-treated to PBS-treated mice. We considered genes significant when they changed by >50%, had a *P*-value <0.05, and had an average occurrence greater than one count per cell across the conditions. The expression of β-actin (*Actb*) was comparable across samples (Supplementary Fig. 7), which suggests that the observed differences were not due to sample variability. We then entered the list of all upregulated genes that met our criteria into the DAVID database[34] and performed an unbiased enrichment analysis. When comparing 20α and PBS, we found an enrichment in genes related to receptor-mediated endocytosis (GO:0006898, 18 of 265 genes, $P < 1.7 \times 10^{-7}$), endocytosis (GO:0006897, 67 of 679 genes, $P < 6.4 \times 10^{-9}$) and endocytic recycling (GO:0032456, 10 of 74 genes, $P < 2.3 \times 10^{-2}$) gene ontology (GO) terms. We also found enriched genes from the cellular response to the low-density lipoprotein particle stimulus pathway (GO:0071404; 7 of 22 genes, $P < 4.1 \times 10^{-3}$). To substantiate the GO results, we performed Kyoto Encyclopedia of Genes and Genomes (KEGG) pathway analysis[35]; this unbiased approach also highlighted genes related to endocytosis (108 of 181 genes, $P < 1.7 \times 10^{-10}$). When comparing 20mix and PBS, we found an enrichment in genes related to endocytosis (GO:0006897, 46 of 679 genes, $P < 2.0 \times 10^{-4}$) and, notably, observed an enrichment in genes related to inflammatory response (GO:0006954, 99 of 727 genes, $P < 2.2 \times 10^{-11}$) and phagocytosis (GO:0006909, 19 of 362 genes, $P < 3.4 \times 10^{-5}$). When performing KEGG pathway analysis comparing 20mix to PBS, we also noted that genes associated with the phagosome (59 of 152 genes, $P < 1.6 \times 10^{-6}$) and lysosome (55 of 152 genes, $P < 7.6 \times 10^{-11}$) were highly enriched. The GO and KEGG analyses led us to two preliminary conclusions: first, that pathways related to LNP uptake and processing were upregulated in LNP-treated mice, relative to PBS-treated mice, independent of cholesterol stereochemistry; and second, that the difference in delivery between 20α and 20mix LNPs could be due to increased inflammation in response to the 20mix LNP, leading to phagocytosis and lysosomal degradation.

The data above did not exclude the possibility that differences in LNP-mediated mRNA delivery were due to endocytosis or maturation of mRNA in late endosomes. We therefore evaluated whether the difference observed between the two LNPs could be due to different receptor-mediated endocytosis pathways. Specifically, exogeneous mRNA endocytosis often occurs via clathrin- or caveolin-mediated processes, but the relative impact of these pathways on LNP delivery in vivo remains understudied[36]. We therefore generated a heatmap representing the expression of three established genes for clathrin- and caveolin-mediated endocytosis, respectively *Clta*, *Cltb*, *Cltc*, *Cav1*, *Cav2* and *Cav3* (Fig. 3a) for both 20α and 20mix, relative to PBS. We observed that Kupffer cells endocytosed LNPs via clathrin-mediated endocytosis only, while endothelial cells endocytosed via both pathways with an inclination for clathrin-mediated endocytosis (Fig. 3a). We did not observe any differences in mechanism between 20α and 20mix. Thus, while these data reveal that the upregulation of genes related to clathrin- and caveolin-mediated endocytosis can vary with cell type in vivo, they did not support the hypothesis that the difference in functional delivery observed between the two LNPs was due to different receptor-mediated endocytosis mechanisms.

We then evaluated whether the difference in delivery was driven by endosomal maturation. Specifically, we reasoned that 20mix LNPs could be trapped in the late endosomes more than 20α LNPs. We evaluated the difference in gene expression of *Eaa1*, which marks the early endosome[37], and *Rab-7*, which marks the late endosome[38]. We generated a heatmap comparing the expression of those genes in each cluster, including their abundance within the cluster, with the expression of Cre mRNA (Fig. 3b and Supplementary Fig. 8) for both 20α and 20mix, relative to PBS. We observed that *Rab-7* was more enriched than *Eea1* in clusters where Cre mRNA was found. These in vivo data are consistent with in vitro data demonstrating that mRNA can be processed by the late endosome[39,40]. However, once again we did not observe any differences between 20α and 20mix; thus, these data do not support our hypothesis that the delivery changes were caused by differential processing in late endosomes (Fig. 3b and Supplementary Fig. 8).

Stereochemistry-dependent LNP trafficking

After excluding the possibility that the difference between Cre mRNA biodistribution and downstream Cre protein activity was explained by endocytosis pathways or endosomal maturation, we returned to the data that implicated phagocytosis and lysosomal degradation as a mechanism. We performed a differential expression analysis, this time comparing 20mix directly to 20α. Once again, we considered genes significant when they changed by >50%, had a *P*-value <0.05 and had an average occurrence greater than one count per cell across the conditions. Among the most upregulated genes found in 20mix, when compared to 20α, were *Mrc1*, *Laptm4a* and *Tsg101*. We represented the differential expression, in 20α and 20mix, of those genes using t-SNE plots (Fig. 3c–e). We observed increased gene expression, particularly in endothelial and Kupffer cells, which was noteworthy, since *Mrc1* can be critical for receptor-mediated endocytosis and phagocytosis[41], while *Laptm* genes regulate lysosomal function and degradation[42]. Finally, previous work has demonstrated that biomolecules can be sorted for lysosomal degradation via *Tsg101* (ref. [43]).

These data led us to postulate that 20mix LNPs were sorted into phagocytic pathways, resulting in different functional delivery between stereopure and non-stereopure LNPs. To further evaluate this hypothesis, we computationally pooled the transcriptomes for each condition to create an aggregate analysis and examined the differentially expressed genes between the three conditions (Fig. 3f and Supplementary Fig. 9). We again considered genes significant when they changed

Fig. 3 | The cellular response to 20α and 20mix LNPs. a, Heatmap representing the expression of three established genes for both clathrin-mediated endocytosis (*Clta*, *Cltb*, *Cltc*) and caveolin-mediated endocytosis (*Cav1*, *Cav2*, *Cav3*) for both 20α and 20mix, relative to PBS. **b**, Heatmap comparing the gene expression of *Eea1* and *Rab-7* in each cluster, including their abundance within the cluster, with the expression of Cre mRNA for 20α, relative to PBS. **c**–**e**, t-SNE plots representing the differential expression, in 20α and 20mix, of *Mrc1* (**c**), *Laptm4a* (**d**) and *Tsg101* (**e**). **f**, Transcriptomes for each condition were computationally pooled to create an aggregate analysis and the differentially expressed genes examined between the three conditions. A volcano plot was used to show the differential expression, between 20mix and 20α, of specific genes related to lysosomal degradation and phagocytosis. **g**, Heatmap comparing the gene expression of several TLRs in each cluster, including their abundance within the cluster, for both 20α and 20mix, relative to PBS. **h**,**i**, 20α (**h**) and 20mix (**i**) LNPs were formulated with a fluorescently tagged and chemically modified mRNA encoding Cre and injected intravenously at 0.3 mg per kg (body weight). Three hours later, livers were isolated, fixed with PFA and cryosectioned. Cells were then stained for the endosomal markers Rab5 and Rab7, and the percentage of mRNA trapped in endosomal compartments was quantified using Manders's overlap coefficient in 25 or more cells per condition. Scale bars, 4 μm.

https://doi.org/10.1038/s41557-023-01138-9

by >50%, had a *P*-value <0.05 and had an average occurrence greater than one count per cell across the condition. First, we compared 20α and 20mix to the PBS-treated control. Notably, none of the significantly differentially expressed genes observed in 20α (43 genes) were also observed in 20mix (11 genes). The differential cell response to both LNPs was further emphasized when comparing the transcriptional profile of 20mix relative to 20α; using the KEGG analytical tool, we once again found that genes from pathways related to phagocytosis

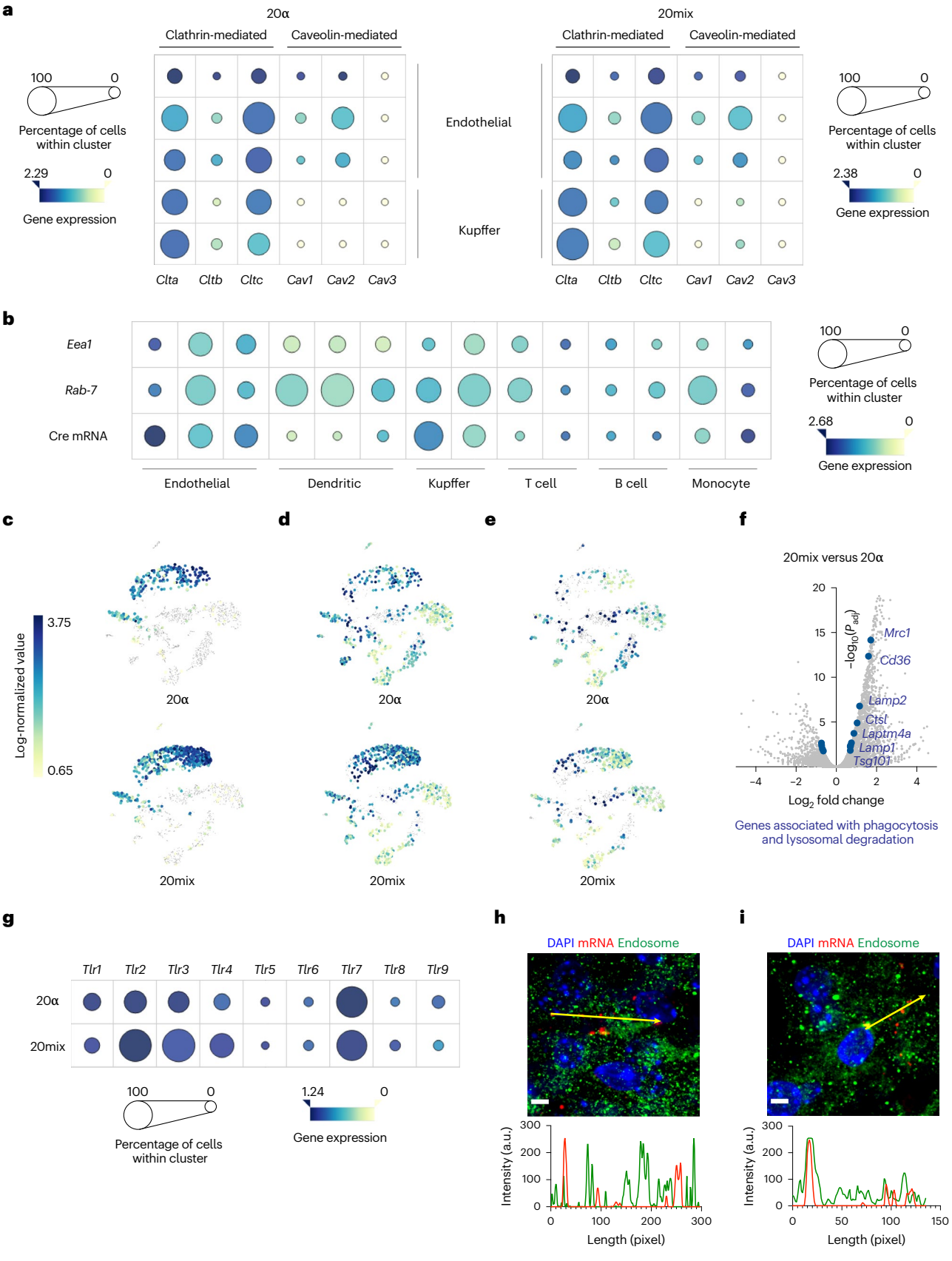

https://doi.org/10.1038/s41557-023-01138-9

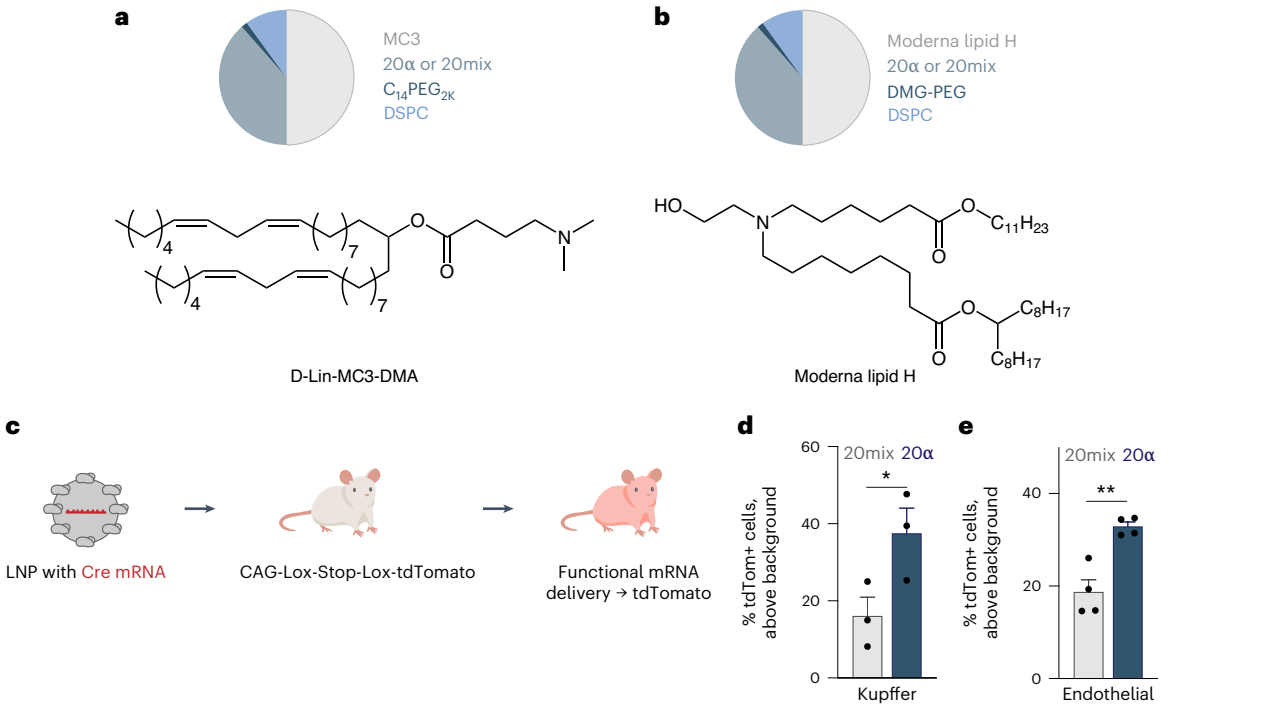

Fig. 4 | Stereochemistry-dependent mRNA delivery is not LNP specific. **a**, 20α- or 20mix-modified MC3-based LNP formulation. **b**, 20α- or 20mix-modified Moderna lipid H-based LNP formulation. **c**, LNPs were formulated to carry chemically modified mRNA encoding Cre recombinase and intravenously administered to Ai14 mice at 0.3 mg per kg (body weight). Cells within Ai14 mice contain a CAG-Lox-Stop-Lox-tdTomato construct. These cells become tdTomato$^+$ (tdTom$^+$) when Cre mRNA is delivered into the cytoplasm and translated into the functional Cre protein, which edits the genome by excising the Stop cassette. **d**, Three days after injection of MC3-based LNPs, we quantified the percentage of tdTom$^+$ Kupffer cells using flow cytometry. $n = 3$ per group, average ± s.e.m. Two-way ANOVA, $^*P = 0.042$. **e**, Three days after injection of Moderna lipid H-based LNPs, we quantified the percentage of tdTom$^+$ liver endothelial cells using flow cytometry. $n = 3$ per group, average ± s.e.m. Two-way ANOVA, $^{**}P = 0.003$.

(9 of 152 genes, $P < 2.4 \times 10^{-6}$) and lysosomes (8 of 181 genes, $P < 4.9 \times 10^{-7}$) were upregulated in cells treated with 20mix, compared to cells treated with 20α (Fig. 3f). When comparing 20mix and PBS, we noted that genes associated with regulation of chronic and acute inflammation, *S100a9* and *S100a8* (GO:0050727; $P < 9 \times 10^{-5}$), were strongly downregulated when the particle was present. *S100a9* and *S100a8* encode co-dependent, calcium-binding proteins; their signalling is believed to play a critical role in mediating inflammatory processes within the plasma membrane through the activation of receptor for advanced glycation end products (RAGE) and Toll-like receptor 4 (TLR4)[44]. We therefore went back to our scRNA-Seq data analysis and investigated the gene expressions of different TLRs in 20α and 20mix, both relative to PBS (Fig. 3g). Analysis of *Tlr1*–*Tlr9* showed that only *Tlr2*, *Tlr3*, *Tlr4* and *Tlr7* were enriched in both LNP-treated conditions. However, the gene expression of *Tlr2*, *Tlr3* and *Tlr4* was found in higher concentration in 20mix, whereas *Tlr7* was slightly more represented in 20α. We previously observed that TLR4 activation reduces LNP delivery of mRNA[13]. Added to our previous analyses, we further hypothesized that stereochemistry affects the sorting of LNPs containing endosomes to phagocytic pathways through the recognition and activation of TLRs.

To evaluate this proposed mechanism using a non-sequencing method in vivo, we formulated 20α and 20mix with a fluorescently tagged and chemically modified mRNA encoding Cre and injected them intravenously at 0.3 mg per kg (body weight). Three hours later, we isolated livers, fixed them with paraformaldehyde (PFA) and cryosectioned them. Cells were then stained for the endosomal markers Rab5 and Rab7 (Fig. 3h,i and Supplementary Fig. 10a), and the percentage of mRNA trapped in endosomal compartments was quantified using Manders's overlap coefficient in 25 or more cells per condition[33,45]. An accumulation of mRNA was observed in the endosomal compartment with 20mix; only 39% of free mRNA was measured compared to 69% with 20α (Supplementary Fig. 10b). Notably, the percentage of free mRNA measured with microscopy was comparable to the average delivery observed for both LNPs across all hepatic cells (68% and 39% for 20α and 20mix, respectively; Fig. 1e). This suggests that Cre mRNA reaching the cytoplasm was translated into protein in similar proportions for both 20α and 20mix; it is therefore unlikely that the disparity in delivery potency was driven by differences in protein translation efficacy. Furthermore, these imaging data, which demonstrate that an increased amount of mRNA is present in the endosomal compartment of cells treated with 20mix, relative to 20α, are consistent with the sequencing data, and support the hypothesis that a shift towards a phagocytic phenotype is responsible for the stereochemistry-dependent differences in delivery.

To evaluate whether stereochemistry-dependent mRNA delivery was specific to one LNP, we quantified the functional delivery of two clinically relevant liver-targeting LNPs. We formulated LNPs containing DLin-MC3-DMA[46] (MC3) or a Moderna[47] ionizable lipid, using either 20α or 20mix (Fig. 4a,b). LNPs were intravenously administered to Ai14 mice at 0.3 mg per kg (body weight) (Fig. 4c). Three days after injection, we quantified the percentage of tdTom$^+$ liver non-parenchymal cells using flow cytometry. We observed a 2-fold increased delivery in Kupffer cells with 20α, relative to 20mix, with MC3 (Fig. 4d) and a 2-fold increased delivery in endothelial cells with 20α, relative to 20mix, with the Moderna lipid (Fig. 4e).

Discussion

Chemists improve small-molecule drugs in part by tuning stereochemistry. Here we provide evidence that similar efforts may improve LNP-mediated mRNA delivery in vivo. These data, which include LNP

biodistribution to cells, subsequent mRNA-mediated protein production and the cellular response to LNPs with single-cell resolution, led us to several conclusions. First, cells exposed to 20α LNPs respond differently from cells exposed to 20mix LNPs. Given that the LNP composition was consistent except for cholesterol stereochemistry, these data suggest that cells can sense or react to differences in LNP stereochemistry. Notably, 20α and 20mix LNPs exhibited similar biophysical traits, suggesting that overt changes in size did not drive the effect. Second, these data suggest that the mechanism is biological, and that specifically, 20mix LNPs tended to lead to higher phagocytic and proinflammatory gene expression. Researchers have observed that phagocytosis can disrupt LNP activity in vitro[48]; our in vivo data support these observations. We previously observed that TLR activation can reduce functional LNP delivery; pre-emptively increasing TLR4 activity reduces LNP delivery, and blocking this activity with a small-molecule inhibitor can rescue the effect[13]. Our third observation was that 20mix biodistribution was higher than 20α biodistribution, yet 20mix protein delivery was lower than 20α protein delivery. These data reinforce the concept that biodistribution is necessary, but not sufficient, for functional RNA delivery, and that it is critical to measure where the LNP payload goes and, separately, where the LNP payload exerts its biological effect on the cell. Finally, we compared 20α-containing LNPs to 20β-containing LNPs, and found that 20β-containing LNPs delivered mRNA less efficiently in vivo (Supplementary Fig. 11).

It is important to acknowledge the limitations of this study. First, while the cell signalling data were generated in vivo, the data were generated in mice. Given that the relationship between LNP delivery and species requires additional study[36], it is feasible that in vivo studies in non-human primates or clinical trials in humans could lead to different results. Second, it remains unclear whether similar stereopurity design rules will apply to polymeric nanoparticles[49], extracellular vesicles[50], PEG10 (ref. [51]) and other non-viral delivery systems. Finally, both LNPs did not efficiently transfect cells in culture. This is consistent with the fact that in vitro and in vivo nanoparticle delivery can poorly predict one another[52]; LNPs that work well in vivo may not work well in vitro. Despite these caveats, these data provide evidence for an important concept: the number of stereocentres and the ability to synthesize and purify a stereopure product should be considered when LNPs are designed.

Online content

Any methods, additional references, Nature Portfolio reporting summaries, source data, extended data, supplementary information, acknowledgements, peer review information; details of author contributions and competing interests; and statements of data and code availability are available at https://doi.org/10.1038/s41557-023-01138-9.

References

1. Brooks, W. H., Guida, W. C. & Daniel, K. G. The significance of chirality in drug design and development. *Curr. Top. Med. Chem.* **11**, 760–770 (2011).
2. Vargesson, N. Thalidomide-induced teratogenesis: history and mechanisms. *Birth Defects Res. C Embryo Today* **105**, 140–156 (2015).
3. Budau, M., Hancu, G., Rusu, A., Carcu-Dobrin, M. & Muntean, D. L. Chirality of modern antidepressants: an overview. *Adv. Pharm. Bull.* **7**, 495–500 (2017).
4. Nguyen, L. A., He, H. & Pham-Huy, C. Chiral drugs: an overview. *Int. J. Biomed. Sci.* **2**, 85–100 (2006).
5. Taechalertpaisarn, J. et al. Correlations between secondary structure– and protein–protein interface-mimicry: the interface mimicry hypothesis. *Org. Biomol. Chem.* **17**, 3267–3274 (2019).
6. Fischer, P. M. The design, synthesis and application of stereochemical and directional peptide isomers: a critical review. *Curr Protein Pept. Sci.* **4**, 339–356 (2003).
7. Akinc, A. et al. Targeted delivery of RNAi therapeutics with endogenous and exogenous ligand-based mechanisms. *Mol. Ther.* **18**, 1357–1364 (2010).
8. Sago, C. D. et al. Modifying a commonly expressed endocytic receptor retargets nanoparticles in vivo. *Nano Lett.* **18**, 7590–7600 (2018).
9. Sahay, G. et al. Efficiency of siRNA delivery by lipid nanoparticles is limited by endocytic recycling. *Nat. Biotechnol.* **31**, 653–658 (2013).
10. Gilleron, J. et al. Image-based analysis of lipid nanoparticle-mediated siRNA delivery, intracellular trafficking and endosomal escape. *Nat. Biotechnol.* **31**, 638–646 (2013).
11. Wittrup, A. et al. Visualizing lipid-formulated siRNA release from endosomes and target gene knockdown. *Nat. Biotechnol.* **33**, 870–876 (2015).
12. Patel, S. et al. Boosting intracellular delivery of lipid nanoparticle-encapsulated mRNA. *Nano Lett.* **17**, 5711–5718 (2017).
13. Lokugamage, M. P. et al. Mild innate immune activation overrides efficient nanoparticle-mediated RNA delivery. *Adv. Mater.* **32**, e1904905 (2019).
14. Paunovska, K., Loughrey, D. & Dahlman, J. E. Drug delivery systems for RNA therapeutics. *Nat. Rev. Genet.* **23**, 265–280 (2022).
15. Adams, D. et al. Patisiran, an RNAi therapeutic, for hereditary transthyretin amyloidosis. *N. Engl. J. Med.* **379**, 11–21 (2018).
16. Gillmore, J. D. et al. CRISPR-Cas9 in vivo gene editing for transthyretin amyloidosis. *N. Engl. J. Med.* **385**, 493–502 (2021).
17. Polack, F. P. et al. Safety and efficacy of the BNT162b2 mRNA Covid-19 vaccine. *N. Engl. J. Med.* **383**, 2603–2615 (2020).
18. Baden, L. R. Efficacy and safety of the mRNA-1273 SARS-CoV-2 vaccine. *N. Engl. J. Med.* **384**, 403–416 (2020).
19. Dong, Y. et al. Lipopeptide nanoparticles for potent and selective siRNA delivery in rodents and nonhuman primates. *Proc. Natl Acad. Sci. USA* **111**, 3955–3960 (2014).
20. Chen, D. et al. Rapid discovery of potent siRNA-containing lipid nanoparticles enabled by controlled microfluidic formulation. *J. Am. Chem. Soc.* **134**, 6948–6951 (2012).
21. Paunovska, K. et al. Nanoparticles containing oxidized cholesterol deliver mRNA to the liver microenvironment at clinically relevant doses. *Adv. Mater.* **31**, e1807748 (2019).
22. Kauffman, K. J. et al. Rapid, single-cell analysis and discovery of vectored mRNA transfection in vivo with a loxP-flanked tdTomato reporter mouse. *Mol. Ther. Nucleic Acids* **10**, 55–63 (2018).
23. Duran-Frigola, M. et al. Extending the small-molecule similarity principle to all levels of biology with the Chemical Checker. *Nat. Biotechnol.* **38**, 1087–1096 (2020).
24. Sirci, F. et al. Comparing structural and transcriptional drug networks reveals signatures of drug activity and toxicity in transcriptional responses. *NPJ Syst. Biol. Appl.* **3**, 23 (2017).
25. Daniszewski, M. et al. Single cell RNA sequencing of stem cell-derived retinal ganglion cells. *Sci. Data* **5**, 180013 (2018).
26. Chen, S., Lake, B. B. & Zhang, K. High-throughput sequencing of the transcriptome and chromatin accessibility in the same cell. *Nat. Biotechnol.* **37**, 1452–1457 (2019).
27. Klein, A. M. et al. Droplet barcoding for single-cell transcriptomics applied to embryonic stem cells. *Cell* **161**, 1187–1201 (2015).
28. Zheng, G. X. et al. Massively parallel digital transcriptional profiling of single cells. *Nat. Commun.* **8**, 14049 (2017).
29. Sommerfeld, S. D. et al. Interleukin-36γ-producing macrophages drive IL-17-mediated fibrosis. *Sci. Immunol.* **4**, eaax4783 (2019).
30. Damm, E. M. et al. Clathrin- and caveolin-1-independent endocytosis: entry of simian virus 40 into cells devoid of caveolae. *J. Cell Biol.* **168**, 477–488 (2005).

31. Wytinck, N. et al. Clathrin mediated endocytosis is involved in the uptake of exogenous double-stranded RNA in the white mold phytopathogen *Sclerotinia sclerotiorum*. *Sci. Rep.* **10**, 12773 (2020).
32. Lorenz, C. et al. Protein expression from exogenous mRNA: uptake by receptor-mediated endocytosis and trafficking via the lysosomal pathway. *RNA Biol.* **8**, 627–636 (2011).
33. Kirschman, J. L. et al. Characterizing exogenous mRNA delivery, trafficking, cytoplasmic release and RNA–protein correlations at the level of single cells. *Nucleic Acids Res.* **45**, e113 (2017).
34. Huang da, W., Sherman, B. T. & Lempicki, R. A. Systematic and integrative analysis of large gene lists using DAVID bioinformatics resources. *Nat. Protoc.* **4**, 44–57 (2009).
35. Kanehisa, M., Furumichi, M., Tanabe, M., Sato, Y. & Morishima, K. KEGG: new perspectives on genomes, pathways, diseases and drugs. *Nucleic Acids Res.* **45**, D353–D361 (2017).
36. Hatit, M. Z. C. et al. Species-dependent in vivo mRNA delivery and cellular responses to nanoparticles. *Nat. Nanotechnol.* **17**, 310–318 (2022).
37. Mu, F. T. et al. EEA1, an early endosome-associated protein. EEA1 is a conserved α-helical peripheral membrane protein flanked by cysteine 'fingers' and contains a calmodulin-binding IQ motif. *J. Biol. Chem.* **270**, 13503–13511 (1995).
38. Vanlandingham, P. A. & Ceresa, B. P. Rab7 regulates late endocytic trafficking downstream of multivesicular body biogenesis and cargo sequestration. *J. Biol. Chem.* **284**, 12110–12124 (2009).
39. Cioni, J. M. et al. Late endosomes act as mRNA translation platforms and sustain mitochondria in axons. *Cell* **176**, 56–72.e15 (2019).
40. Herrera, M., Kim, J., Eygeris, Y., Jozic, A. & Sahay, G. Illuminating endosomal escape of polymorphic lipid nanoparticles that boost mRNA delivery. *Biomater. Sci.* **9**, 4289–4300 (2021).
41. Garcia-Aguilar, T., Espinosa-Cueto, P., Magallanes-Puebla, A. & Mancilla, R. The mannose receptor is involved in the phagocytosis of mycobacteria-induced apoptotic cells. *J. Immunol. Res.* **2016**, 3845247 (2016).
42. Vergarajauregui, S., Martina, J. A. & Puertollano, R. LAPTMs regulate lysosomal function and interact with mucolipin 1: new clues for understanding mucolipidosis type IV. *J. Cell Sci.* **124**, 459–468 (2011).
43. Jovic, M., Sharma, M., Rahajeng, J. & Caplan, S. The early endosome: a busy sorting station for proteins at the crossroads. *Histol. Histopathol.* **25**, 99–112 (2010).
44. Markowitz, J. & Carson, W. E. 3rd Review of S100A9 biology and its role in cancer. *Biochim. Biophys. Acta* **1835**, 100–109 (2013).
45. Tiwari, P. M. et al. Engineered mRNA-expressed antibodies prevent respiratory syncytial virus infection. *Nat. Commun.* **9**, 3999 (2018).
46. Jayaraman, M. et al. Maximizing the potency of siRNA lipid nanoparticles for hepatic gene silencing in vivo. *Angew. Chem.* **51**, 8529–8533 (2012).
47. Hassett, K. J. et al. Optimization of lipid nanoparticles for intramuscular administration of mRNA vaccines. *Mol. Ther. Nucleic Acids* **15**, 1–11 (2019).
48. Gustafson, H. H., Holt-Casper, D., Grainger, D. W. & Ghandehari, H. Nanoparticle uptake: the phagocyte problem. *Nano Today* **10**, 487–510 (2015).
49. Piotrowski-Daspit, A. S., Kauffman, A. C., Bracaglia, L. G. & Saltzman, W. M. Polymeric vehicles for nucleic acid delivery. *Adv. Drug Deliv. Rev.* **156**, 119–132 (2020).
50. Herrmann, I. K., Wood, M. J. A. & Fuhrmann, G. Extracellular vesicles as a next-generation drug delivery platform. *Nat. Nanotechnol.* **16**, 748–759 (2021).
51. Segel, M. et al. Mammalian retrovirus-like protein PEG10 packages its own mRNA and can be pseudotyped for mRNA delivery. *Science* **373**, 882 (2021).
52. Paunovska, K. et al. A direct comparison of in vitro and in vivo nucleic acid delivery mediated by hundreds of nanoparticles reveals a weak correlation. *Nano Lett.* **18**, 2148–2157 (2018).

Methods

Synthesis

Both cKK-E12[19] and 20mix[53] were synthesized according to literature procedures (Supplementary Fig. 12). Starting materials, reagents and solvents were purchased from commercial sources (Sigma Aldrich) and used as received unless stated otherwise. Purification of reaction products was carried out according to standard laboratory methods. Thin-layer chromatography was carried out using Merck silica plates coated with fluorescent indicator UV254. Thin-layer chromatography plates were analysed under 254 nm ultraviolet light or developed using potassium permanganate solution. ^{1}H spectra were acquired on a Varian Mercury Vx 400 spectrometer at 400 MHz. ^{13}C NMR spectra were acquired on a Varian Mercury Vx 400 spectrometer at 100 MHz. High-resolution mass spectra (HRMS) were obtained through analysis at the Bioanalytical Mass Spectrometry Facility at Georgia Institute of Technology.

Compound characterization

(3*S*,6*S*)-3,6-Bis(4-(bis(2-hydroxydodecyl)amino)butyl) piperazine-2,5-dione (cKK-E12). ^{1}H NMR (400 MHz, $CDCl_3$) δ (ppm) 4.02 (br s, 2H), 3.71 (br s, 4H), 3.06–2.19 (m, 12H), 1.86 (br s, 4H), 1.43–1.21 (m, 80H), 0.87 (t, J = 8 Hz, 12H). HRMS-ESI, m/z calculated $[M + 2H]^{2+}$ for $C_{60}H_{121}O_6N_4$ 497.4677, found 497.4662; m/z calculated $[M + H]^{+}$ for $C_{60}H_{121}O_6N_4$ 993.9272, found 993.9281 (Supplementary Figs. 13 and 14).

(8*S*,9*S*,10*R*,13*S*,14*S*,17*S*)-17-(2-Hydroxy-6-methylhepta n-2-yl)-10,13-dimethyl-2,3,4,7,8,9,10,11,12,13,14,15,16,17-tetr adecahydro-1*H*-cyclopenta[a]phenanthren-3-ol (20mix). The configuration of the diastereomers of compound 20mix was assigned according to a literature report[54] based on the chemical shifts of C-20 and H3-21 (singlet). The C-20 chemical shift of the 20*S* diastereomer is around 75.40 ppm while it is 75.97 ppm for 20*R*, and the H3-21 chemical shift of the 20*S* diastereomer is around 1.26 ppm while it is 1.11 ppm for 20*R* (Supplementary Figs. 15–17). HRMS-ESI, m/z calculated $[M + Na]^{+}$ for $C_{27}H_{46}O_2$ 425.3382, found 425.3390.

Cre mRNA synthesis

mRNA was synthesized as described previously[45]. Briefly, the Cre mRNA sequence was ordered as a plasmid from GeneArt (Thermo Fisher Scientific) containing a 5′ untranslated region (UTR) with Kozak sequence, a 3′ UTR derived from the mouse α-globin sequence, and the open reading frame sequence, which was human codon optimized using the GeneArt website. Plasmids were digested into a linear template using NotI-HF (New England BioLabs) overnight at 37 °C. Linearized templates were purified by ammonium acetate (Thermo Fisher Scientific) precipitation before being resuspended with nuclease-free water. In vitro transcription was performed overnight at 37 °C using the HiScribe T7 kit (New England BioLabs) following the manufacturer's instructions (full replacement or uracil with *N*1-methyl-pseudouridine). RNA product was treated with DNase I (Aldevron) for 30 min to remove template and purified using lithium chloride precipitation (Thermo Fisher Scientific). RNA transcripts were heat denatured at 65 °C for 10 min before being capped with a Cap1 structure using guanylyl transferase (Aldevron) and 2′-*O*-methyltransferase (Aldevron). Transcripts were then polyadenylated enzymatically (Aldevron). mRNA was then purified by lithium chloride precipitation, treated with alkaline phosphatase (New England BioLabs) and purified a final time. Concentrations were measured using a NanoDrop, and mRNA stock concentrations were between 2 and 5 mg ml^{-1}. mRNA stocks were stored at −80 °C. Purified RNA products were analysed by gel electrophoresis to ensure purity.

Nanoparticle formulation

Nucleic acids, DNA barcodes and mRNA were diluted in 10 mM citrate buffer (Teknova). Lipid-amine compound cKK-E12, $C_{14}PEG_{2000}$ (Avanti, 880150), 20α and DOPE were diluted in 100% ethanol. Both phases were loaded into separate syringe pumps. The citrate and ethanol phase were mixed in a microfluidic device. All PEGs and cholesterols were purchased from Avanti Lipids.

Nanoparticle characterization

This method is reproduced from a previous publication[55]. LNP hydrodynamic diameter was measured using high-throughput dynamic light scattering (DynaPro Plate Reader II, Wyatt). LNPs were diluted in sterile 1× PBS and analysed. To avoid using unstable LNPs, and to enable sterile purification using a 0.22 µm filter, LNPs were included only if they met three criteria: diameter >20 nm, diameter <200 nm and correlation function with one inflection point. Particles that met these criteria were dialysed with 1× PBS.

Animal experiments

This method is reproduced from a previous publication[55]. All animal experiments were performed in accordance with the Georgia Institute of Technology's Institutional Animal Care and Use Committee. All animals were bred in the Georgia Institute of Technology Animal Facility. C57BL/6 J (#000664) were purchased from The Jackson Laboratory. LSL-Tomato/Ai14 (#007914) were purchased from The Jackson Laboratory for breeding proposes. In all experiments, we used n = 3–5 mice per group. Mice were injected intravenously via the lateral tail vein. The nanoparticle concentration was determined using NanoDrop (Thermo Scientific).

Cell isolation and staining

Cells were isolated 72 h after injection with LNPs unless otherwise noted. Mice were perfused with 20 ml of 1× PBS through the right atrium. Liver tissues were finely minced, and then placed in a digestive enzyme solution with collagenase type I (Sigma Aldrich), collagenase XI (Sigma Aldrich) and hyaluronidase (Sigma Aldrich) at 37 °C at 550 r.p.m. for 45 min[56,57]. The cell suspension was filtered through 70 µm mesh and red blood cells were lysed. Cells were stained to identify specific cell populations and sorted using the BD FacsFusion and BD Facs Aria IIIu cell sorters in the Georgia Institute of Technology Cellular Analysis Core. The antibody clones used were the following: anti-CD31 (390, BioLegend), anti-CD45.2 (104, BioLegend), anti-CD68 (FA11, BioLegend), anti-CD11c (N418, Biolegend) and PE anti-mCD47 (miap301, BioLegend). Representative flow gates are shown in Supplementary Fig. 1. PBS-injected Ai14 mice were used to gate tdTomato populations for intravenous administration.

Droplet Digital polymerase chain reaction

This method is modified from a previous publication[55]. Droplet Digital polymerase chain reaction (ddPCR) reads were analysed using the QX200 Droplet Digital PCR system. ddPCR samples were prepared with 10 µl ddPCR Supermix for Probes (Bio-Rad), 1 µl of primer/probe mix, 1 µl of template/TE buffer and 8 µl water. Then 20 µl and 70 µl of Droplet Generation Oil for Probes (Bio-Rad) were loaded into DG8 cartridges and covered with gaskets.

2-(*p*-Toluidino)-6-naphthalene sulfonic acid assay

This method is modified from a previous publication[58]. First, 10 mM HEPES, 10 mM MES, 10 mM sodium acetate and 140 nM sodium chloride (all Sigma) were pH adjusted between 4 and 10. Then, 140 µl buffer, 5 µl of 2-(*p*-toluidino)-6-naphthalene sulfonic acid (60 µg ml^{-1}) and 5 µl of each LNP were added to a 96-well plate. After 5 min of incubation, fluorescence absorbance was measured using excitation/emission wavelengths of 325/435 nm.

Single-cell RNA-Seq library construction and sequencing

Samples were isolated and prepared as described above. Individually barcoded single-cell RNA-Seq libraries were prepared using the Chromium instrument and the Single Cell 3′ Reagent kit (v.3) following

the manufacturer's protocol (10X Genomics). Approximately 2,000 cells were loaded for each of the three conditions. The quantity and quality of the libraries were examined with a Qubit DNA BR Assay Kit, a Qubit3.0 Fluorometer (Life Technologies) and an Agilent 2100 Bioanalyzer (Agilent Technologies). Library sequencing was performed on an Illumina NextSeq platform, using the 150-cycle High Output kit (Illumina).

Bioinformatics analysis for single-cell RNA-Seq

Sample demultiplexing, barcode processing and single-cell 3′ gene counting were performed with the Cell Ranger Single Cell Software Suite CR3.0.2. Each droplet partition's contents were tagged with a unique molecule identifier, which was read as the second read of each sequenced read-pair, along with Illumina barcodes. Ninety-eight nucleotides of Read1s were aligned to the mouse genome (mm10) using the STAR aligner. Only confidently mapped non-PCR duplicates with valid barcodes and unique molecule identifiers were used for further analysis (>97%). A read is considered exonic if at least 50% of it intersects an exon, intronic if it is non-exonic and intersects an intron, and intergenic otherwise. To compare single-cell populations, the Cell Ranger matrix file was imported into Seurat and processed using the previously described workflow[59]. In summary, cells were log normalized to a scale factor of 10,000 then scaled using a linear transformation. This was followed by principal component analysis dimensionality reduction and t-SNE clustering, and the cells were then exported using rBCS for further analysis in BBrowser2 (v.2.9.23). Once in Bbrowser2, the cell search tool was used to identify the cell types within each cluster, and gene expression profiles were compared within cell types of interest.

Aggregate RNA analysis

To find differentially expressed genes between groups of cells, the asymptotic beta test used in edgeR[60] was used. For each cluster, the algorithm is run on that cluster versus all other cells, yielding lists of genes that are differentially expressed in that cluster relative to the rest of the sample. Only genes with a *P* adjusted value (false-discovery rate) of <0.05 and a fold change >1.5, and genes that have an average occurrence >1 count per cell across the condition, were included within the subsequent GO and KEGG pathway analyses. To understand the functions of the differentially expressed genes, GO functional enrichment and KEGG pathway analyses were carried out by the Enrichr web server[61] and KEGGMapper (https://www.kegg.jp/), respectively.

Microscopy

mRNA was fluorescently labelled four 2′-*O*-methyl RNA-DNA chimeric oligonucleotides, complementary to four adjacent sequences across the 3′ UTR region, with the following sequences: MT1: T(C6-amino)-TTTTT-T(C6-amino)-MeOG-MeOC-MeOA-MeOA-MeOG-MeOC-MeOC-MeOC-MeOCMeOG-MeOC-MeOA-MeOG-MeOA-MeOA-MeOG-MeOG-T(C6-amino). MT2: T(C6-amino)-TTATTT(C6-amino)-MeOA-MeOG-MeOA-MeOG-MeOA-MeOA-MeOG-MeOA-MeOA-MeOG-MeOG-MeOGMeOC-MeOA-T(C6-amino)-MeOG-MeOG. MT3: T(C6-amino)-TTTT-T(C6-amino)-A-MeOC-MeOCMeOA-MeOA-MeOG-MeOA-MeOG-MeOG-T(C6-amino)-MeOA-MeOC-MeOA-MeOG-MeOG-T(C6-amino)-MeOG-MeOC. MT4: T(C6-amino)-TTTTTT-MeOC-T(C6-amino)-MeOA-MeOC-MeOU-MeOCMeOA-MeOG-MeOG-MeOC-T(C6-amino)-MeOU-MeOU-MeOA-MeOU-T(C6-amino)-MeOC (Biosearch Technologies). The oligos were fluorescently labelled by conjugating Dylight 650 NHS-ester (Thermo Fisher Scientific) to the amino-modified thymidines following the manufacturer's instructions, followed by purification with 10 kDa filters (Amicon, Fisher Scientific) to remove unbound dyes. In vitro transcribed mRNA was buffer exchanged into 1× PBS and combined with linear oligos in a 1:0.7 molar ratio. mRNA labelling with fluorescently labelled probes was performed in a thermal cycler by heating the sample at 70 °C and gradually decreasing the temperature to room temperature in 1 °C min steps^{-1}. Labelled mRNA was formulated into LNPs and delivered to mice as described.

LSL-Tomato/Ai14 (#007914) were injected with 0.3 mg per kg (body weight (of Cre mRNA total dose. In all experiments, we used $n = 3–5$ mice per group. Mice were injected intravenously via the lateral tail vein. Mice were perfused with 20 ml of 1× PBS through the right atrium. Livers were isolated after 3 h and fixed with 8% PFA (Electron Microscopy Sciences). Livers were fixed in 4% PFA overnight followed by treatment with 30% sucrose overnight before OCT embedding and cryosectioning. Tissue section slides were incubated in antigen retrieval buffer (Dako) for 15 min on steam followed by cooling at room temperature for 20 min. The slides were incubated in PBST for 10 min, blocked with PBST containing 5% donkey serum and 1% BSA for 1 h, and finally incubated with the following primary antibodies: rabbit anti-Rab5 (Thermo Fisher, 1:250) and rabbit anti-Rab7 (Abcam, 1:250). Next, the slides were washed three times with PBST and incubated with the secondary antibodies Alexa Fluor 488 donkey anti-rabbit or donkey anti-mouse (Thermo Fisher, 1:250) for 1 h at room temperature in PBST containing 5% donkey serum and 1% BSA. Finally, the slides were washed three times with PBST, nuclei were counterstained with 4,6-diamidino-2-phenylindole and the slides were mounted with Prolong Gold. Images were acquired with a Hamamatsu Flash 4.0 v.2 sCMOS camera on a PerkinElmer UltraView spinning disk confocal microscope mounted to a Zeiss Axiovert 200M body with a 63× numerical aperture 1.4 Plan-Apochromat objective. Images were acquired with Volocity (PerkinElmer) with *z* stacks taken in 0.2 µm increments. Image acquisition and analysis was performed using the Volocity software (PerkinElmer). Twenty-five or more cells were analysed per experimental condition on at least two independent samples.

Reporting summary

Further information on research design is available in the Nature Portfolio Reporting Summary linked to this article.

Data availability

All RNA sequencing data are available at GEO (GSE181333). All other data are represented in the main figures or supplementary figures.

Code availability

All code used to analyse the data is available at https://github.com/Jack-Feldman/barcode_count.

References

53. Nedelcu, D., Liu, J., Xu, Y., Jao, C. & Salic, A. Oxysterol binding to the extracellular domain of Smoothened in Hedgehog signaling. *Nat. Chem. Biol.* **9**, 557–564 (2013).
54. Nachtergaele, S. et al. Oxysterols are allosteric activators of the oncoprotein Smoothened. *Nat. Chem. Biol.* **8**, 211–220 (2012).
55. Gan, Z. et al. Nanoparticles containing constrained phospholipids deliver mRNA to liver immune cells in vivo without targeting ligands. *Bioeng. Transl. Med.* **5**, e10161 (2020).
56. Dahlman, J. E. et al. In vivo endothelial siRNA delivery using polymeric nanoparticles with low molecular weight. *Nat. Nano.* **9**, 648–655 (2014).
57. Sager, H. B. et al. RNAi targeting multiple cell adhesion molecules reduces immune cell recruitment and vascular inflammation after myocardial infarction. *Sci. Transl. Med.* **8**, 342ra380 (2016).
58. Sago, C. D. et al. Nanoparticles that deliver RNA to bone marrow identified by in vivo directed evolution. *J. Am. Chem. Soc.* **140**, 17095–17105 (2018).
59. Satija, R., Farrell, J. A., Gennert, D., Schier, A. F. & Regev, A. Spatial reconstruction of single-cell gene expression data. *Nat. Biotechnol.* **33**, 495–502 (2015).

60. Robinson, M. D., McCarthy, D. J. & Smyth, G. K. edgeR: a Bioconductor package for differential expression analysis of digital gene expression data. *Bioinformatics* **26**, 139–140 (2010).
61. Kuleshov, M. V. et al. Enrichr: a comprehensive gene set enrichment analysis web server 2016 update. *Nucleic Acids Res.* **44**, W90–W97 (2016).

Acknowledgements

The authors thank S. Durham, R. Hughley, D. Gulick, N. Djeddar at Georgia Tech, and D. Alexis at the Emory Winship Cancer Institute. The authors thank K. Tiegren. This work was funded by the National Institutes of Health (R01GM132985, awarded to J.E.D., and UG3-TR002855, awarded to J.E.D. and P.J.S.).

Author contributions

M.Z.C.H., C.Z., P.J.S. and J.E.D. designed the experiments. All authors helped to perform the experiments. M.Z.C.H. and J.E.D. wrote the initial draft, which was sent to the other authors.

Competing interests

J.E.D. is an advisor to GV. All other authors declare no competing interests.

Additional information

Supplementary information The online version contains supplementary material available at https://doi.org/10.1038/s41557-023-01138-9.

Correspondence and requests for materials should be addressed to James E. Dahlman.

Peer review information *Nature Chemistry* thanks Hideyoshi Harashima and the other, anonymous, reviewer(s) for their contribution to the peer review of this work.

nature research

Corresponding author(s): James Dahlman

Last updated by author(s): Oct 30, 2022

Reporting Summary

Nature Research wishes to improve the reproducibility of the work that we publish. This form provides structure for consistency and transparency in reporting. For further information on Nature Research policies, see our Editorial Policies and the Editorial Policy Checklist.

Statistics

For all statistical analyses, confirm that the following items are present in the figure legend, table legend, main text, or Methods section.

n/a	Confirmed	
☐	☒	The exact sample size (*n*) for each experimental group/condition, given as a discrete number and unit of measurement
☐	☒	A statement on whether measurements were taken from distinct samples or whether the same sample was measured repeatedly
☐	☒	The statistical test(s) used AND whether they are one- or two-sided *Only common tests should be described solely by name; describe more complex techniques in the Methods section.*
☒	☐	A description of all covariates tested
☒	☐	A description of any assumptions or corrections, such as tests of normality and adjustment for multiple comparisons
☐	☒	A full description of the statistical parameters including central tendency (e.g. means) or other basic estimates (e.g. regression coefficient) AND variation (e.g. standard deviation) or associated estimates of uncertainty (e.g. confidence intervals)
☐	☒	For null hypothesis testing, the test statistic (e.g. *F*, *t*, *r*) with confidence intervals, effect sizes, degrees of freedom and *P* value noted *Give P values as exact values whenever suitable.*
☒	☐	For Bayesian analysis, information on the choice of priors and Markov chain Monte Carlo settings
☒	☐	For hierarchical and complex designs, identification of the appropriate level for tests and full reporting of outcomes
☒	☐	Estimates of effect sizes (e.g. Cohen's *d*, Pearson's *r*), indicating how they were calculated

Our web collection on statistics for biologists contains articles on many of the points above.

Software and code

Policy information about availability of computer code

Data collection	In vivo cell populations were analyzed and isolated using the BD FacsFusion in the Georgia Institute of Technology Cellular Analysis Core. Sequencing data was collected with an Illumina NextSeq High Throughput Flow Cell or a Chromium Controller 10X Genomics.
Data analysis	Data were analyzed in GraphPad Prism. The specifics of the data analyses are described in the text. Flow cytometry data was analyzed using FlowJo. Sequencing data were analyzed using BBrowser2.

For manuscripts utilizing custom algorithms or software that are central to the research but not yet described in published literature, software must be made available to editors and reviewers. We strongly encourage code deposition in a community repository (e.g. GitHub). See the Nature Research guidelines for submitting code & software for further information.

Data

Policy information about availability of data

All manuscripts must include a data availability statement. This statement should provide the following information, where applicable:

- Accession codes, unique identifiers, or web links for publicly available datasets
- A list of figures that have associated raw data
- A description of any restrictions on data availability

All RNA sequencing data are available at GEO (GSE181333). All code used to analyze the data is available (https://github.com/Jack-Feldman/barcode_count). All other data are represented in the main figures or supplementary figures.

Field-specific reporting

Please select the one below that is the best fit for your research. If you are not sure, read the appropriate sections before making your selection.

☒ Life sciences ☐ Behavioural & social sciences ☐ Ecological, evolutionary & environmental sciences

For a reference copy of the document with all sections, see nature.com/documents/nr-reporting-summary-flat.pdf

Life sciences study design

All studies must disclose on these points even when the disclosure is negative.

Sample size	For in vivo experiments: N = 2 for PBS negative control and 3 or 4 mice for experimental control. Those sample sizes were chosen to ensure the accuracy of the data and accurate statistics. The 2 mice per PBS control were chosen to limit the number of mice. No statistical method was used to predetermine sample size.
Data exclusions	No data were excluded from the analyses.
Replication	LNPs were confirmed at least three times independently and successfully.
Randomization	Mice were randomly selected, and no algorithm was used.
Blinding	The Investigators were not blinded to allocation during experiments and outcome assessment. Blinding investigators was not necessary to perform this research

Reporting for specific materials, systems and methods

We require information from authors about some types of materials, experimental systems and methods used in many studies. Here, indicate whether each material, system or method listed is relevant to your study. If you are not sure if a list item applies to your research, read the appropriate section before selecting a response.

Materials & experimental systems

n/a	Involved in the study
☐	☒ Antibodies
☒	☐ Eukaryotic cell lines
☒	☐ Palaeontology and archaeology
☐	☒ Animals and other organisms
☒	☐ Human research participants
☒	☐ Clinical data
☒	☐ Dual use research of concern

Methods

n/a	Involved in the study
☒	☐ ChIP-seq
☐	☒ Flow cytometry
☒	☐ MRI-based neuroimaging

Antibodies

Antibodies used	The antibody clones used were the following: anti-CD31 (390, BioLegend), anti-CD45.2 (104, BioLegend), anti-CD68 (FA11, BioLegend), anti-CD11c (N418, Biolegend), and PE anti-mCD47 (miap301, BioLegend).
Validation	anti-CD31 (BioLegend, 390): "Anti-mouse CD31 clones 390 and MEC13.3 bind to their respective non-overlapping epitopes in IgD2 of CD31. CD31 is a 130-140 kD glycoprotein, also known as platelet endothelial cell adhesion molecule (PECAM-1) and EndoCAM". anti-CD45.2 (BioLegend, 104): "CD45.2 is an alloantigen of CD45, expressed by Ly5.2 bearing mouse strains (e.g., A, AKR, BALB/c, CBA/Ca, CBA/J, C3H/He, C57BL, C57BR, C57L, C58, DBA/1, DBA/2, NZB, SWR, 129). CD45, a member of the protein tyrosine phosphatase (PTP) family, is a 180-240 kD glycoprotein expressed on all hematopoietic cells except mature erythrocytes and platelets." anti-CD68 (FA11, BioLegend): "CD68 is an 85-115 kD member of the lysosomal-associated membrane protein (LAMP) family. It is expressed on tissue macrophages, Langerhans cells and at low levels on dendritic cells." anti-CD11c (N418, Biolegend): "CD11c is a 150 kD glycoprotein also known as αX integrin, CR4, and p150. It is primarily expressed on dendritic cells, NK cells, a subset of intestinal intraepithelial lymphocytes (IEL), and some activated T cells." anti-mCD47 (miap301, BioLegend): "CD47, also known as Integrin-Associated Protein (IAP), is a membrane protein of about 50 kD with an IgV-like extracellulaur domain, a five membrane-spanning segment and a short terminal cytoplasmic region. It is widely expressed on many cell types and often associated with beta 3 integrins."

Animals and other organisms

Policy information about studies involving animals; ARRIVE guidelines recommended for reporting animal research

Laboratory animals	LSL-Tomato/Ai14 (#007914) were purchased from The Jackson Laboratory for breeding proposes. All mice were 6 to 8 weeks old at

Laboratory animals	the time of experiments. Both males and females were used. Light cycle of mice housing room are from 7 am to 7 pm. Housing room are kept at ~ 70 F with ~ 30% average humidity.
Wild animals	None
Field-collected samples	None
Ethics oversight	All animal experiments were performed in accordance with the Georgia Institute of Technology's Institutional Animal Care and Use Committee's animal care and services policy.

Note that full information on the approval of the study protocol must also be provided in the manuscript.

Flow Cytometry

Plots

Confirm that:

☒ The axis labels state the marker and fluorochrome used (e.g. CD4-FITC).

☒ The axis scales are clearly visible. Include numbers along axes only for bottom left plot of group (a 'group' is an analysis of identical markers).

☒ All plots are contour plots with outliers or pseudocolor plots.

☒ A numerical value for number of cells or percentage (with statistics) is provided.

Methodology

Sample preparation	Cells were isolated 72 hours after injection with LNPs unless otherwise noted. Mice were perfused with 20 mL of 1X PBS through the right atrium. Liver tissues were finely minced, and then placed in a digestive enzyme solution with Collagenase Type I (Sigma Aldrich), Collagenase XI (Sigma Aldrich) and Hyaluronidase (Sigma Aldrich) at 37 ºC at 550 rpm for 45 minutes60, 61. Cell suspension was filtered through 70Eim mesh and red blood cells were lysed. Cells were stained to identify specific cell populations and sorted using the BD FacsFusion and BD Facs Aria IIIu cell sorters in the Georgia Institute of Technology Cellular Analysis Core.
Instrument	BD FacsFusion and BD Facs Aria IIIu
Software	The data were analyzed using FlowJo (BD Biosciences)
Cell population abundance	Greater than 1000.
Gating strategy	Cells were gated on FSC-A / SSC-A. Singlets were gated FSC-A / FSC-H. Cells types were gated by CD31 / CD45.2 then on CD68 / CD11c. PBS mice were used to gate tdTomato positive cells. See supporting figure 1 for additional information.

☒ Tick this box to confirm that a figure exemplifying the gating strategy is provided in the Supplementary Information.